Conformation of Poly(styrene sulfonate) Layers Physisorbed from High Salt Solution Studied by Force Measurements on Two Different Length Scales

Stephan Block and Christiane A. Helm*

Institut für Physik, Ernst-Moritz-Arndt Universität, Felix-Hausdorff-Str. 6, D-17487 Greifswald, Germany

Received: March 9, 2008; Revised Manuscript Received: May 6, 2008

The conformation of poly(styrene sulfonate) (PSS) layers physisorbed from 1 M NaCl is determined by force measurements and imaging on two length scales. With colloidal probe technique steric forces as predicted for neutral grafted brushes are observed. On decrease and increase of the NaCl concentration, the grafting density remains constant, yet the brush thickness swells and shrinks reversibly with the salt concentration with an exponent of −0.3. At low salt conditions, the brush length amounts to 30% of the contour length, a behavior known for polyelectrolyte brushes and attributed to the entropy of the counterions trapped in the brush. Between a PSS layer and a pure colloidal silica sphere, the same steric forces are observed, and additionally at large separations (beyond the range of the steric repulsion) an electrostatic force is found. A negatively charged AFM tip penetrates the brush—a repulsive electrostatic force between the tip and surface is found, and single chains can be imaged. Thus, with the nanometer-sized AFM tip, the flatly adsorbed fraction of the PSS chains is seen, whereas the micrometer-sized colloidal probe interacts with the fraction of the chains penetrating into solution.

Introduction

Adsorbed polyelectrolytes are used in a multitude of traditional applications (e.g., as wet and dry strength additives, as flocculating or dispersing agents) but also in basic research in connection with material and the life sciences. Polyelectrolyte multilayers made by sequential adsorption of alternately charged polyions are used for optics, electronics, membranes, etc.[1–6] Therefore, to understand the conformation of the polyelectrolytes as well as surface forces is of major importance.

From various measurements, it is well-known that polyelectrolytes adsorbed from salt-free solutions exhibit a flat conformation accompanied by surface charge overcompensation, as has been established theoretically[7,8] and experimentally.[9–11] However, in most cases, polyelectrolytes are adsorbed from salt solutions of intermediate or high ionic strength to increase the amount of adsorbed polyelectrolyte.[12,13] It is not known how the increase in surface coverage influences the polyelectrolyte conformation.

We showed last year that linear polyelectrolytes physisorbed from 1 M NaCl solution exhibit a nonflat conformation.[14] Surface forces between such layers were described with the theory of Alexander and de Gennes[15] for anchored neutral polymers. This is a behavior very different from polyelectrolytes adsorbed from salt-free solution, which show an electrostatic repulsion.[16–18] While for linear polyelectrolytes adsorbed from high salt concentration no electrostatic force was directly observed, the thickness of the physisorbed layer scales like a salted brush (this is one of the phases occurring in polyelectrolyte brushes and is characterized by incorporation of counterions into the brush leading to charge neutralization within the brush). Therefore, we concluded that in the presence of 1 M NaCl linear polyelectrolytes adsorb in a coiled conformation onto the surface. Parts of the chains dangle into solution (leading to high surface coverage and steric forces), and surprisingly, these chains show some properties known for neutral brushes even though the brush thickness scales as a polyelectrolyte brush.

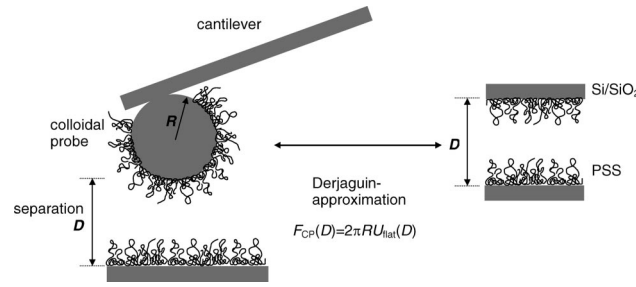

Figure 1. Setup of the colloidal probe technique: A colloidal probe (CP) with radius R is glued to the end of a cantilever, and the force F_{CP} acting between the CP and a surface is measured by applying Hooke's law to the deflection. For small surface separations ($D \ll R$), this force normalized by $2\pi R$ gives the interaction energy per unit area U_{flat} of the same but flat surfaces.

However, the Alexander de Gennes theory was originally derived to describe the force acting between two surfaces with end-grafted neutral polymer brushes, and the relevance for physisorbed polyelectrolytes is not obvious. Further corroboration is necessary. One of the assumptions of the Alexander de Gennes theory is a boxlike brush profile. Other theories like the Milner, Witten, Cates assume a parabolic polymer profile.[19] The respective force curves are rather similar: a steep increase of the force at small surface separations and an exponential decay at intermediate separations with a decay length proportional to the brush thickness L. On further separation of the surfaces, the force curves differ. The steplike decrease of the brush segment density of the Alexander de Gennes theory leads to a steep decrease of the surface forces, whereas the parabolic profile of the Milner, Witten, Cates theory leads to a slower decline. To distinguish the respective force curves, it is necessary to measure both small and large forces, i.e., to resolve 3 orders

* Corresponding author.

10.1021/jp8020672 CCC: $40.75
Published on Web 07/12/2008

TABLE 1: Four Different Surface Sets Used in the Experiment and the Purpose of the Measurement, Together with the Respective Spring Constants of the Cantilevers Used

Surface Sets and Experiments Performed			
set	symmetric cantilever spring constant	asymmetric cantilever spring constant	purpose
S1	$k = 28.2$ mNm^{-1}	–	CP: symmetric force profiles, behavior on drying
S2	$k = 34.4$ mNm^{-1}	–	
S3	$k = 40.7$ mNm^{-1}	$k = 22.0$ mNm^{-1}	CP: symmetric and asymmetric force profiles
S4	$k = 31.9$ mNm^{-1}	$k = 28.2$ mNm^{-1} $k = 5.14$ mNm^{-1}	CP: symmetric and asymmetric force profiles, behavior on drying
	–	$k = 60.1$ mNm^{-1} $k = 62.2$ mNm^{-1}	tip: PSS layer penetration

of magnitude. This was achieved by averaging over at least 200 force curves. An additional advantage of the good resolution is a reduced error of the grafting density.

To probe the stability of the PSS conformation on the substrate surface, the physisorbed PSS layers were dried for a few days, then were immersed into 1 M NaCl solutions, and the surface forces were determined.

To further validate the description of the adsorbed polyelectrolyte layer as neutral brush, asymmetric surfaces were investigated. One surface is covered with PSS physisorbed from 1 M NaCl, and the other surface is either a colloidal probe as received or a standard AFM tip. Since both the colloid surface and the AFM tip are negatively charged,[20] we hope to gain further insight into the electrostatic forces which cause the strong chain stretching. To probe the lateral homogeneity, it was tried to penetrate the PSS layer with an AFM tip. We show that in asymmetric force measurements, both steric and electrostatic forces can be found and that their magnitude strongly depends on the dimension of the probe.

To investigate the chain conformation on the surface, the AFM tip was used to image the surfaces. One might imagine that the chains adsorb as slightly deformed coils, with few anchoring points on the surface, or the chains adsorb flatly and cause a reversal of the surface charge (as is known from polyelectrolytes adsorbed from salt-free solution), with some isolated chains protruding into the solution. To address these questions, tapping mode images were taken at different salt concentrations.

Materials

All solutions were created with ultrapure water using a Milli-Q device (Millipore, Billerica, MA). Poly(styrene sulfonate) (PSS, 350 kDa, contour length $L_C = 425$ nm) was obtained from Polymer Standard Service (Mainz, Germany), NaCl and P_2O_5 from Merck (Darmstadt, Germany), and 3-aminopropyldimethyl-ethoxysilane from ABCR (Karlsruhe, Germany). All chemicals were used without further purification. The PSS deposition solution was prepared by solving 1 M NaCl and 3 mM PSS monomers in Milli-Q water.

For the colloidal probe technique, cantilevers CSC12 (spring constant $k = 0.005-0.04$ N/m) were bought from MicroMasch (Tallin, Estonia) and silica spheres from Bangs Laboratories (Fishers, IN; radius $R = 3$ μm). Layer penetration was performed using D-NP cantilevers (curvature radius <60 nm), whereas for imaging, we used "sharper" D-NPS cantilevers (curvature radius <20 nm), both obtained from Veeco (France).

Surface Preparation. Microscope slides (Roth, Karlsruhe, Germany) were used as silica surfaces, cleaned according to the RCA standard, and freshly used. Colloidal probes (CPs) were created by gluing silica spheres onto the cantilevers using a UV-cureable epoxy (NOA68, Norland Adhesives, Cranbury, NJ) and cleaned with argon-plasma at 35 W for 5 min (Harrick Scientific, NY). The surfaces (intended for PSS adsorption) were positively charged by silanization (several days in an argon-silane atmosphere) and coated with PSS by physisorption from 1 M NaCl solution for 1 h at 30 °C. After adsorption, the surfaces were directly transferred (i.e., without drying) into the fluid cell of our commercial DI Multimode AFM with a Nanoscope IIIa Controller (Santa Barbara, CA). For asymmetric measurements and imaging, bare CPs or tips were cleaned with argon-plasma at 35 W for 5 min and directly used.

Force Measurements. The setup of the colloidal probe technique is sketched in Figure 1a. The force measurements were performed in deposition solution or in PSS-free NaCl solutions of different ionic strengths: starting at 1 M, then diluting down to 1 mM, and enriching again to 1 M. Force curves were recorded not later than five minutes after change of the solution. We performed symmetric measurements (both surfaces covered with PSS) as well as asymmetric measurements (one PSS covered surface against a bare silica CP or a silicon tip). During one experiment, we recorded at least 200 force curves for each salt concentration at different positions on the surface, with one approach/separation cycle per five seconds. Shown are only the averaged force curves. Afterward, the spring constants were determined using the methods of Butt, Sader, and Cleveland.[21–23]

Furthermore, the surfaces were dried either at ambient conditions (approximately 25% r.h.) or at 0% r.h. (P_2O_5 inside an exsiccator).

Imaging. For imaging, a silicon surface was used which is much flatter than silica (rms-roughness, determined with tapping mode, of about 1.7 Å compared to 4.0 Å), but we prepared the PSS layers as described before. The morphology was measured using tapping mode in PSS-free NaCl solutions of different ionic strengths (between 1 M and 1 mM NaCl as indicated).

Experiments. Table 1 summarizes the performed experiments. Four different sets of surfaces (silica plus colloidal probe) were created. All measurements were repeated at least with two different sets of surfaces. All in all, more than 40 000 force curves were recorded.

Theory

Forces between Neutral Polymer Brushes. De Gennes extended the theory of Alexander to describe the steric force acting between two end-grafted neutral polymer brushes (called AdG theory below[15]). He showed that for a brush with thickness L and grafting density $\Gamma = s^{-2}$ the repulsive pressure between two plane surfaces is given by

$$P_{\mathrm{AdG,symm}}(D) = \frac{k_B T}{s^3}\left[\left(\frac{2L}{D}\right)^{\frac{9}{4}} - \left(\frac{D}{2L}\right)^{\frac{3}{4}}\right] \quad \text{for } D < 2L \quad (1)$$

Here, D denotes the surface separation and s is called the average distance between grafting points. Three important assumptions are used within this model: (1) the brushes are end-grafted, (2) the brushes do not interpenetrate, and (3) the volume fraction profile of the undisturbed brush is constant within the brush and zero elsewhere.

Using the first assumption, it follows that every brush has only one grafting point and only one tail. Therefore, one can reinterpret s as average distance between adjacent tails. This is important, because the steric force is generated by the interaction of opposing tails and not of grafting points, and hence for adsorbed polyelectrolytes, the parameter s gives information about the density of tails and loops. Below we will summarize both loops and tails by the term pseudotails.[24]

O'Shea et al. used the assumed lack of brush interpenetration to show that this theory can be successfully applied to describe the interaction of a polymer brush with a bare, nonadsorbing surface.[25] They concluded that this asymmetric case can be described with eq 1 by replacing $2L$ by L and dividing eq 1 by 2 leading to[26]

$$P_{\mathrm{AdG,asymm}}(D) = \frac{k_B T}{2s^3}\left[\left(\frac{L}{D}\right)^{\frac{9}{4}} - \left(\frac{D}{L}\right)^{\frac{3}{4}}\right] \quad (2)$$

Milner et al. used a parabolic volume fraction profile of the brush instead of the steplike profile assumed by Alexander and de Gennes and calculated

$$P_{\mathrm{MWC,symm}}(D) = \frac{k_B T L_C}{2L}\left(\frac{\pi^2 l_p}{12 s^{10}}\right)^{\frac{1}{3}}\left[-\left(\frac{D}{2L}\right)^{-2} + 2\left(\frac{D}{2L}\right) - \left(\frac{D}{2L}\right)^4\right] \quad \text{for } D < 2L \quad (3)$$

as pressure acting between two polymer brush covered surfaces (called MWC theory below).[19] Here L_C denotes the contour length and l_p the persistence length. Using the same reasoning as above leads to the pressure in the asymmetric case[26]

$$P_{\mathrm{MWC,asymm}}(D) = \frac{k_B T L_C}{4L}\left(\frac{\pi^2 l_p}{12 s^{10}}\right)^{\frac{1}{3}}\left[-\left(\frac{D}{L}\right)^{-2} + 2\left(\frac{D}{L}\right) - \left(\frac{D}{L}\right)^4\right] \quad \text{for } D < L \quad (4)$$

In 1934, Derjaguin showed that the force between a flat and a curved surface of radius R can be related to the interaction energy per unit area $W(D)$ of two flat surfaces by[27]

$$F(D) = 2\pi R \cdot W(D)$$

as long as the length scale of the force and the observed surface separation D is much smaller than R (cf. Figure 1).

To apply the theories to measurements with colloidal probes, one has to integrate the respective pressures

$$\frac{F_{\mathrm{AdG,symm}}(D)}{2\pi R} = \frac{8 k_B T L}{35 s^3} \cdot \left[7\left(\frac{2L}{D}\right)^{\frac{5}{4}} + 5\left(\frac{D}{2L}\right)^{\frac{7}{4}} - 12\right] \quad (5a)$$

$$\frac{F_{\mathrm{AdG,asymm}}(D)}{2\pi R} = \frac{2 k_B T L}{35 s^3} \cdot \left[7\left(\frac{L}{D}\right)^{\frac{5}{4}} + 5\left(\frac{D}{L}\right)^{\frac{7}{4}} - 12\right] \quad (5b)$$

$$\frac{F_{\mathrm{MWC,symm}}(D)}{2\pi R} = k_B T L_C\left(\frac{\pi^2 l_p}{12 s^{10}}\right)^{\frac{1}{3}} \cdot \left[\left(\frac{D}{2L}\right)^{-1} + \left(\frac{D}{2L}\right)^2 - \frac{1}{5}\left(\frac{D}{2L}\right)^5 - \frac{9}{5}\right] \quad (5c)$$

and

$$\frac{F_{\mathrm{MWC,asymm}}(D)}{2\pi R} = \frac{k_B T L_C}{4}\left(\frac{\pi^2 l_p}{12 s^{10}}\right)^{\frac{1}{3}} \cdot \left[\left(\frac{D}{L}\right)^{-1} + \left(\frac{D}{L}\right)^2 - \frac{1}{5}\left(\frac{D}{L}\right)^5 - \frac{9}{5}\right] \quad (5d)$$

Please note that the removal of one brush layer reduces the prefactor of the force by a factor of 4.

Both force profiles (AdG as well as MWC) are nonlinear functions which can be well approximated at intermediate surface separations ($0.2 \le D/L \le 0.9$) by an exponential function with a decay length given by $\gamma^{-1} = -L/\pi$ (symmetric) and $\gamma^{-1} = -L/2\pi$ (asymmetric), respectively, which depends only on the brush thickness L.[28]

Approach for Determining Zero Surface Separation ($D = 0$). With the colloidal probe technique, the interaction of a colloidal probe with a flat surface is measured. Usually the CP is glued at the end of an AFM cantilever with known spring constant k. From the deflection of the cantilever, one can calculate the force acting on the CP by using Hooke's law. The surface separation (i.e., the distance between the surfaces) is usually calculated with the algorithm described in ref 26 and is set to zero, if the surfaces are in contact.

However, in our case, zero surface separation can never be reached as thick polyelectrolyte layers are adsorbed onto the surfaces. The AdG and MWC force profiles (eq 5) go to infinity as the surface separation reaches zero, and hence there will always be a displacement δ between the surface separation calculated from the data D_{CP} and the true surface separation $D = D_{CP} + \delta$. The proper determination of this displacement is crucial as the fitted value of the grafting density strongly depends on it.

Fortunately, the shape of an AdG force profile is only determined by L, whereas the parameter s only causes a "vertical shift" of the force profile (on logarithmic scales) and the displacement a "horizontal shift". Therefore, it is possible to determine the displacement δ by performing a least-mean squares (LMS) fit of the theoretical force profiles to the measured force profile as long as the steep decline at large separations can be resolved by the measurement (cf. Figure 2). With this method, δ and hence $D = 0$ were determined for all measurements.

Results

Symmetric Force Profiles. Figure 2 shows three representative force profiles at different salt concentrations (symmetric case, i.e., both surfaces covered by PSS physisorbed from 1 M NaCl solution) and fits to the symmetric force profiles by the AdG and the MWC theory, respectively (eq 5). We found no hysteresis between approach and retraction of the surface, and hence only the approach part of the force curve is given in Figure 2.

The force profiles are resolved over 3 orders of magnitude, and a steep decline at large separation is visible. Hence, it is reasonable to perform fits to the AdG (eq 5a) and MWC theories (eq 5c), respectively, to decide which theory describes the force profiles best.

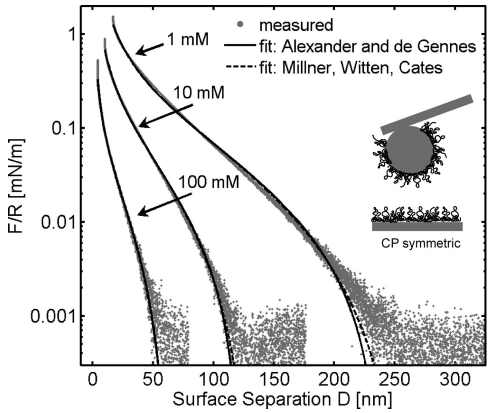

Figure 2. Representative force profiles (gray dots) if both surfaces are covered by PSS (physisorbed from 1 M NaCl solution) at different salt concentrations as indicated by the arrows and the fits to the symmetric force profiles of the AdG and the MWC theory (lines, eq 5a and eq 5c, respectively). Above 10 mM NaCl, there is no noticeable difference between both theories.

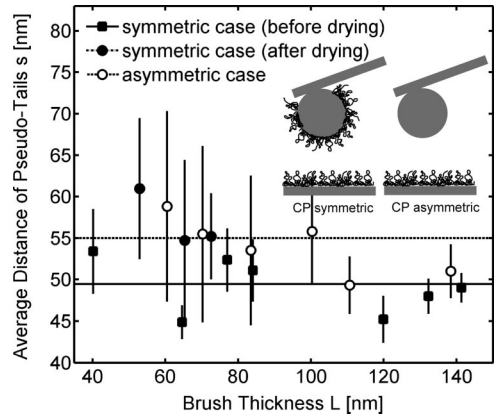

Figure 3. Average pseudotail distance versus brush thickness for all force measurements performed on surface set S4 (cf. Tables S1−S3 in the Supporting Information). The squares correspond to symmetric measurements performed directly after deposition, whereas the circles give the pseudotail distance after drying to 0% r.h. determined in symmetric (full circles) and asymmetric (open circles), respectively, configuration. For each experiment, this distance is constant within experimental error, although the brush thickness changes by 1 order of magnitude. This indicates that pseudotails are neither created nor destroyed. After drying, the average pseudotail distance increases from 50 to 55 nm indicating a minor change in the PSS layer structure. Furthermore, fits to the symmetric and asymmetric data (eq 5a and eq 5b, respectively) yield the same average pseudotail distance.

For the MWC theory, the persistence length l_p was calculated using the formula of Odijk and co-workers:[29,30] $l_p = l_0 + (l_B/4\kappa^2a^2)f[1 - (8/3)Y^{-1} + (e^{-Y}/3)(Y + 5 + 8Y^{-1})]$. Here l_0 denotes the intrinsic persistence length (= 1.2 nm, according to Nierlich et al.[31]), l_B the Bjerrum length ($l_B = e^2/\epsilon k_BT = 0.713$ nm for water at 25 °C), f the effective charge factor (= 0.35, according to refs 32 and 33), κ^{-1} the Debye length (= 0.304 nm/$\sqrt{I}$ for monovalent salts of concentration I), a the linear spacing between charges (= 0.25 nm, which is the monomer spacing in PSS), and Y is defined by $Y = \kappa L_C$.

Figure 2 shows that both theories result in very good fits of the experimental data. The parameters to these fits can be found in Table S1 (in the Supporting Information). Obviously, all parameters are the same for both theories within experimental error. These findings are representative for all symmetric force measurements.

Above 10 mM salt concentration in solution, a difference between the AdG and the MWC theory is (experimentally and numerically) almost not noticeable. Here, the AdG theory is sufficient to describe the force profiles properly, and like in previous measurements, the addition of electrostatic forces is not necessary.[14,36] Hence, the brush appears neutral on the length scale of the CP.

Only below 10 mM NaCl concentration, the force profiles are better described using the MWC theory. The main difference between both theories is the assumed volume fraction profile which indicates that at least below 10 mM the parabolic volume fraction profile (MWC theory) is more realistic than the boxlike one stated by the AdG theory.

As the fits of both theories yield almost equal parameters, we will only show the parameters of the AdG theory below. The AdG parameters for all surface sets can be found in Table S1 (in the Supporting Information) and in Figure 3 (average distance between pseudotails, full circles) and Figure 4 (brush thickness, full circles), respectively, for the symmetric measurements performed on surface set S4 (cf. Table 1). Table S1 shows that there are only minor deviations between different surface sets and that the PSS brush swells from about 20 nm at 1 M NaCl to approximately 140 nm at 1 mM NaCl, which is 1/3 of the contour length (425 nm). In addition, the parameters of the force measurements in deposition solution and in 1 M NaCl do not differ within the experimental error. The removal of the

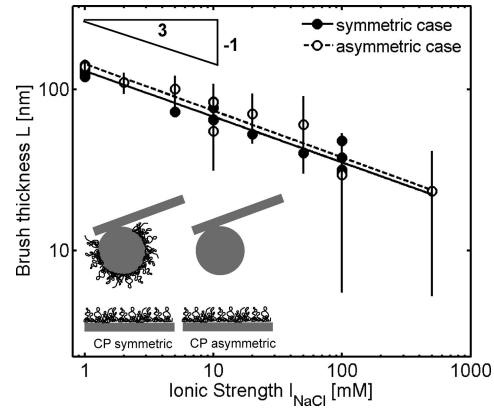

Figure 4. Brush thickness versus ionic strength for all force measurements performed on surface set S4 (symmetric before and after drying to 0% r.h. = filled circles, asymmetric = open circles). The brush swells by roughly a factor of 10 on decrease of the salt concentration and reaches 1/3 of the contour length at 1 mM NaCl. The swelling/shrinking is reversible; i.e., it does not depend on the prior salt concentration. Fits to the symmetric and asymmetric data (eq 5a and eq 5b, respectively) yield the same brush thickness, and in both cases, the brush thickness scales as known for salted polyelectrolyte brushes.

PSS from the adsorption solution does not affect the force profiles, and structural changes of the PSS layer are not observed.

The average distance between pseudotails is constant within the experimental error (cf. Figure 3) but changes by 10% between different sets of surfaces. The steric interaction is created by pseudotails dangling into solution. The constant pseudotail density upon change of salt concentration suggests that pseudotails are neither created nor destroyed; i.e., the chains of the brush do not detach from the surface or form new adsorption points if they are pushed onto the surface by the CP. This is an interesting behavior because Figure 4 shows that the brush swells by roughly a factor of 10, and hence the chains creating the steric interaction have to be stretched also by roughly a factor of 10. This is only possible if some chains are

anchored by strong local bonds at one side and dangle into solution at the other side. Furthermore, they have to be coiled at high salt concentrations and start to stretch upon decrease of the ionic strength.

However, we observe no swelling−shrinking hysteresis (cf. Figure 4); i.e., the force curves do not depend on previous salt concentration. Furthermore, at 1 mM NaCl concentration, a brush thickness of 120 nm is reached which amounts to 30% of the contour length of the PSS. Common theories of polyelectrolyte brushes attribute this strong stretching to an increased electrostatic repulsion of the charged monomers and derive a scaling law for the brush thickness given by

$$L \sim (I_{\mathrm{NaCl}} s^2)^{\alpha}$$

with $\alpha = -1/3$ for the case of salted polyelectrolyte brushes.[34,35] Figure 4 shows that our measurements are consistent with this scaling law as we derive a scaling parameter of $\alpha = -0.3$. This is in good agreement with measurements of other groups; e.g., Tran et al. report a scaling parameter of −0.27, whereas Balastre et al. used an SFA (surface forces apparatus) to show that α can be found between −0.3 and −0.33.[36,37]

Stability of the Brush on Drying. To check the stability of the brush, we performed three experiments where the brush bearing surfaces (i.e., the silica surface and the corresponding CP) were dried at ambient conditions (approximately 25% r.h.) and also at 0% r.h. and afterward reimmersed into a solution of 1 M NaCl. After equilibrating for 1 h, we recorded the force profiles at various salt concentrations. Here, the results are not as uniform as the other measurements.

One of the three surface sets (S2, cf. Table 1) showed forces which we attribute to electrostatic interaction as their decay lengths match the expected Debye length. We infer that here the brush collapsed upon drying and was not able to swell again in solution yielding a quite flat PSS layer.

Another surface set (S4) showed bridging forces at $I_{\mathrm{NaCl}} >$ 0.1 M but restored almost completely the original force profiles (i.e., before drying) at salt concentrations below 0.1 M. This is a surprising fact as polyelectrolyte adsorption and drying are nonequilibrium processes. Furthermore, it was even possible to dry this set two times at ambient r.h. and two times at 0% r.h. over a period of altogether 3 months and regain the original force profiles. The brush thickness at salt concentrations below 50 mM was not affected by the drying process (cf. surface set S4 in Tables S1 and S2 in the Supporting Information).

The average pseudotail distance of this surface set (S4) is given for both cases in Figure 3 (full squares and circles). This plot shows that upon drying the pseudotail distance increases from 50 to 55 nm which decreases the pseudotail density by approximately 20%. From this, we can conclude that after the first drying there is a minor change in the PSS layer structure and that after reimmersing not all chains are able to stretch again.

The third set (S1) showed at salt concentrations $I_{\mathrm{NaCl}} >$ 10 mM forces which we (like in the first case) attribute to electrostatic interaction, but below 10 mM, repulsive forces occurred with a decay length that was in between the electrostatic and steric interaction. Here, it might be that the layer structure was more changed than in the second case but less than in the first case. It appears that the availability of binding places at the surfaces is important, when the chains collapse. Probably, to improve the reproducibility, the silanization needs to be better controlled.

Asymmetric Force Profiles. It was shown in the previous paragraphs that the PSS layer physisorbed from 1 M NaCl exhibits a nonflat conformation (in contrast to PSS physisorbed from salt-free solutions, which adsorbs flatly onto the surface) and that this conformation causes steric forces that can be quantitatively described by force laws derived for neutral end-grafted polymers, while the brush length scales by a power law derived for salted polyelectrolyte brushes. Here, electrostatic forces play no or only a minor role even at salt concentrations (<10 mM NaCl) where electrostatic forces usually dominate the force profile of polyelectrolyte covered surfaces.

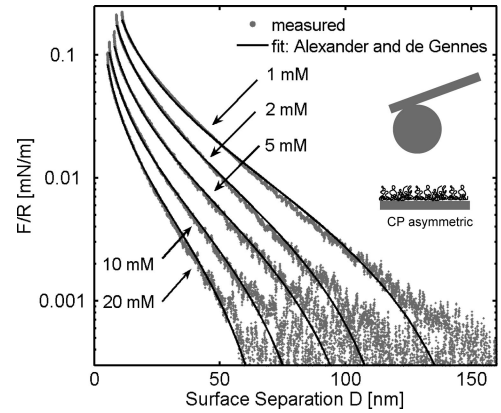

Figure 5. Representative asymmetric force profiles (gray dots) of the surface set S4 at different salt concentrations as indicated by the arrows and the fits to the asymmetric force profiles of the AdG theory (lines, eq 5b). There is an additional repulsive interaction at large separation when the steric interaction vanishes. Therefore, we added an electrostatic contribution to the steric force profile (cf. Figure 7).

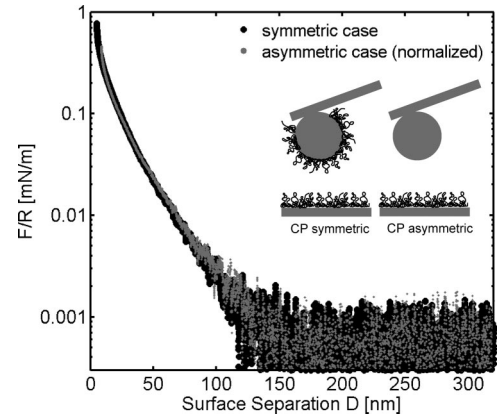

Figure 6. Comparison of a symmetric (black dots) and a normalized asymmetric force profile (gray dots), both recorded at 10 mM NaCl. Since the relevant parameters (s and L) are so similar (cf. Figures 3 and 4), it is easy to superimpose asymmetric and symmetric force curves by normalizing the asymmetric force curve as motivated by theoretical considerations of O'Shea et al. (cf. Forces between Neutral Polymer Brushes and ref 25).

To check if the PSS layer completely behaves as expected for a neutral brush, asymmetric force curves were recorded. The measurement started with the recording of symmetric force profiles as described above. Then the PSS covered CP was replaced by a bare CP, and asymmetric force profiles were measured. By replacing only one of the two surfaces, a direct comparison between symmetric and asymmetric force profiles is possible.

Figure 5 shows five representative asymmetric force profiles at different salt concentrations and the fits to the asymmetric force profiles according to the AdG theory (eq 5b). Here, we omitted fits to the MWC theory as the difference between AdG and MWC is too small to be significant. Again, only the approach part of the force curve is given.

Like the symmetric case (cf. Figure 2), the force profiles are well described by the AdG theory. The parameter plots to these fits are given in Figure 3 (average distance between pseudotails) and Figure 4 (brush thickness). Both plots show a very good agreement of the symmetric and asymmetric parameter sets. Furthermore, we directly compare a symmetric with an asymmetric force profile (cf. Figure 6). The theory predicts that both curves should overlap if the asymmetric force profile is normalized as follows: the surface separation has to be doubled and the amplitude of the force multiplied by a factor of 4. Since the relevant parameters (s and L) are so similar (cf. Figure 3 and 4), it is easy to superimpose asymmetric and symmetric force curves. A representative plot is given in Figure 6 where an excellent match was obtained with a factor of 1.5 (for the surface separation) and 3.6 (for the amplitude). This differs less than 25% from the expected values. Hence, we conclude that the PSS layers completely behave as is expected for a (neutralized) brush; i.e., they satisfy the assumptions made by the AdG theory.

However, Figure 5 shows deviations from the AdG theory at larger surface separations even at 20 mM. At this salt concentration, the symmetric force profiles are well described by the AdG theory, and hence one cannot attribute this deviation to polydispersity or to a different volume fraction profile of the brush as the replacement of one PSS covered surface by a bare one does not change properties of the remaining surface. Figure 5 shows that there is interaction of the surfaces even at surface separations where the steric interaction vanishes. Therefore, we added an electrostatic contribution to the steric force profile.

A charged surface (immersed in an aqueous salt solution of salt concentration I) attracts counterions and repels coions in such a way that the potential decays exponentially. The decay length is called Debye length and is given by $\kappa^{-1} = 0.304\ \text{nm}/\sqrt{I}$ for monovalent salts.[28,38] The overlap of "counterion-clouds" of two approaching (charged) surfaces leads to a rearrangement of the counterion concentration between the surfaces resulting in an increased osmotic pressure and hence in a force repelling the surfaces (called electrostatic force below). For monovalent salts, at surface separations larger than the Debye length and for surface potentials below 25 mV, the osmotic pressure between two flat surfaces can be well described by

$$P_{\mathrm{DL}}(D) = 0.0482\sqrt{I}\kappa \tanh\left[\frac{\psi_{0,1}}{103\ \text{mV}}\right] \tanh\left[\frac{\psi_{0,2}}{103\ \text{mV}}\right] e^{-\kappa D} \tag{6}$$

where $\psi_{0,1/2}$ denotes the respective surface potential at infinite surface separation.[28] This leads (after integration of eq 6 and application of the Derjaguin approximation) to the force profile

$$\frac{F_{DL}(D)}{2\pi R} = 0.0482\sqrt{I} \tanh\left[\frac{\psi_{0,1}}{103\ \text{mV}}\right] \tanh\left[\frac{\psi_{0,2}}{103\ \text{mV}}\right] e^{-\kappa D} \tag{7}$$

At surface separation $D < \kappa^{-1}$, deviations from eqs 6 and 7 might occur due to charge regulation effects of the surfaces[39] or van der Waals forces.[28]

We add an electrostatic contribution to the asymmetric brush force profile using the following approximations: (1) the brush is almost completely neutralized by incorporated counterions (so-called salted brush), (2) the plane of origin of the electrostatic interaction is for one side the top of the brush and for the second side the silica surface of the colloid, (3) the brush behaves as a spring and exhibits a neutral brush force profile, (4) the electrostatic interaction is approximated by the constant potential case; i.e., the surface potentials are constant and eqs 6 and 7 are valid for all surface separations down to contact.

In this model, an increase of the electrostatic interaction (e.g., by decreasing the surface separation) will also increase the osmotic pressure acting on the brush and compress the brush. If L denotes the undisturbed brush height (i.e., at infinite surface separation), D_1 the equilibrium brush height, and D the surface separation, then the equilibrium condition reads $P_{\mathrm{AdG}}(D_1) = P_{\mathrm{DL}}(D - D_1)$, or in other words, the brush is repelled by the surface until steric and electrostatic pressure are equal. One can easily use this condition to compute the complete asymmetric force profile.

We fitted this force profile to asymmetric force measurements as follows: For a given D_1, we calculated with eq 6 the separation D' ($= D - D_1$) between the top of the brush and the bare surface which fulfills $P_{\mathrm{AdG}}(D_1) = P_{\mathrm{DL}}(D')$. Hardcore repulsion was added by setting negative D' to zero because negative values indicate that the steric force is larger than the highest achievable electrostatic force (i.e., at contact, when the PSS brush touches the bare surface). Hence, for the CP measurement, the complete asymmetric force profile is given by $F_{\mathrm{AdG+DL}}(D \equiv D_1 + D'): = F_{\mathrm{DL}}(D')$. The fitting procedure started by performing an LMS fit of the data to the purely steric force profile, eq 5 (as described in the previous paragraph), followed by an LMS fit to $F_{\mathrm{AdG+DL}}(D)$ (keeping the parameters L, s, and δ from the previous fit) to obtain the surface potential $\psi_{0,1} = \psi_{0,\mathrm{PSS}}$. The Debye length used in eqs 6 and 7 was calculated from the salt concentration in the aqueous solution, and the values for the surface potential of the CP $\psi_{0,2} = \psi_{0,\mathrm{SiO_2}}$ used in this fit are given in Table S4 (in the Supporting Information) and were obtained by measurement of the surface forces between two bare silica surfaces and fits to eq 7.

Figure 7 compares two representative asymmetric force profiles (the 1 mM and 20 mM profiles from Figure 5) with fits to the asymmetric AdG theory with (dashed line) and without (dotted line) electrostatic contribution. In all cases, the developed model describes the data almost perfectly, whereas the effect is more obvious at 1 mM than at 20 mM. We attribute this to the fact that at 1 mM the Debye length is more than 4 times larger than at 20 mM, and hence electrostatic effects will lead to stronger deviations at lower salt concentrations. The surface potential of the brush (0.02−0.06 mV, cf. Table S4) shows that in asymmetric CP measurements the electrostatic forces are very weak (small surface potential) and can only be detected at surface separations exceeding $2L$ where the steric force vanishes. On compression of the brush, electrostatic forces cannot be resolved using a CP as the steric interaction exceeds by far any electrostatic contribution.

Asymmetric Force Profiles, AFM Tip. We tried to penetrate the PSS brush by using an AFM tip (curvature radius around 60 nm). Figure 8 shows two representative force profiles recorded at 1 mM and 10 mM which were obtained by averaging the approach part of the measured force curves. These profiles can be directly compared to the asymmetric CP measurements of the previous section because the same PSS brush bearing surface was used. As the Derjaguin approximation cannot be applied to tips with curvature radius less than the interaction range, this figure shows the measured force F instead of the normalized force F/R. Hence the decay length of the force curve can be quantitatively measured but not the magnitude of the force. Here, only a qualitative description is possible (e.g., the sign of the charge).

In Figure 8 (logarithmic plot), the force profiles decay exponentially, with two different slopes. The change of the slope

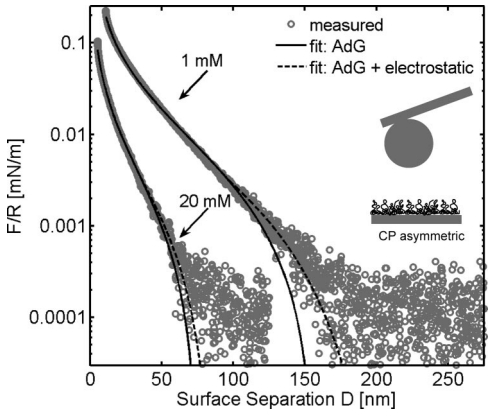

Figure 7. Comparison of two representative asymmetric force profiles (circles, 1 mM and 20 mM profiles from Figure 5) with fits to the asymmetric AdG theory with (dashed line, eq 5b) and without (dotted line) electrostatic contribution.

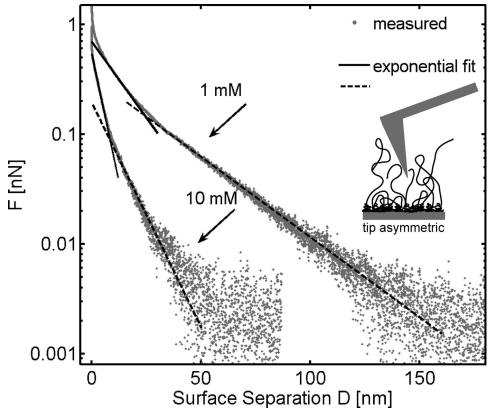

Figure 8. Two representative asymmetric force profiles (gray dots) recorded by penetrating the PSS layer with an AFM tip (curvature radius about 60 nm). The force profile can be well described by two exponential fits (solid and dashed line). The decay length of the more long-ranged interaction (dashed line) matches very well the expected decay length for asymmetric brush interaction in all cases (except for 1 mM NaCl).

occurs at approximately 0.1 nN. The decay length of the more long-ranged interaction (dashed line) matches very well the expected decay length for asymmetric brush interaction in all cases (except for 1 mM NaCl); i.e., the decay lengths obtained here are in very good agreement with the decay lengths (measured at intermediate surface separation) of the data presented in the previous section. Therefore we subtracted this exponential approximation (dashed line) from the force profile, and the result is given in Figure 9. This plot shows that after subtraction the force profile can be well described with an exponential decay which is now resolved over 2 orders of magnitude (compared to Figure 8). The decay length of these force profiles matches very well the expected Debye length (inset), and we infer that this contribution is an electrostatic force.

We conclude that the asymmetric force profiles measured with a sharp tip (instead of a CP) can be well described by the superposition of an electrostatic and a steric contribution, or $F(D) = C_1 e^{-(L/2\pi)D} + C_2 e^{-\kappa D}$. Furthermore, the electrostatic force is the dominant contribution at small surface separations which means that the tip penetrates the brush and the force is created by the interaction of the tip with the bottom of the brush (an interaction of the tip with parts of the brush would lead to strong steric forces at small surface separations, and hence the steric contribution would dominate).

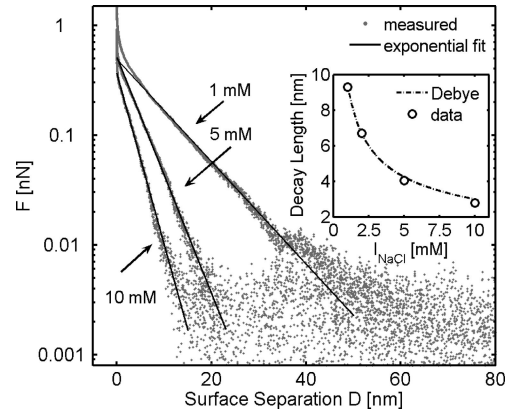

Figure 9. Same asymmetric force profiles as given in Figure 8 (plus the profile for 5 mM) but with the long-range exponential fit (dashed line in Figure 8) subtracted from the force profile. As the decay length perfectly matches the expected Debye length (cf. inset), we infer an electrostatic origin of this contribution.

In addition, the electrostatic contribution is due to the interaction of the tip with a negatively charged surface, i.e., uncoated parts of the silica surface (e.g., due to incomplete silanization), or with PSS adsorbed on silanized parts of the surface, as the interaction of the negatively charged tip with a positively charged surface would lead to attractive forces and to adhesion. Such negative forces cannot be found in the force profiles.

We performed AFM tapping mode imaging of the substrate in air and of the PSS layer in salt solutions to get more information about the surface structure. Previous work showed that silica is too rough for such experiments, and hence we used silicon surfaces instead.[18]

The structure of the silicon surface before and after silanization (data not shown) is flat without any holes or other features and exhibits a roughness of 1.9 Å. After PSS adsorption, the roughness increases to 4.1 Å in 1 M NaCl (cf. Figure 10a), but the surface remains homogeneous and structureless. From this and the lack of attractive forces during brush penetration, we infer that the PSS layer was adsorbed homogeneously on the length-scale of the tip (i.e., several 10 nm). On further decrease of the salt concentration, wormlike structures become visible, which we attribute to PSS chains, and the roughness increases (reaching 5.3 Å at 1 mM NaCl concentration). This process is irreversible: an increase of the salt concentration back to 1 M reduces the roughness only to 4.7 Å, and the difference between both images taken at 1 M NaCl is obvious (cf. Figure 10a before and Figure 10c after dilution) as the PSS chains are still visible.

The height range (about 2 nm for all images) is independent of the salt concentration. This is surprising as all force measurements indicate that range of the force strongly depends on the salt concentration. However, it was shown that the AFM tip is able to penetrate the PSS brush, and hence we are looking at the bottom of the PSS brush. Furthermore, the observed chains are not much more stretched at lower salt concentrations (cf. Figure 10c at 10 mM NaCl) compared to higher concentrations (cf. Figure 10b at 1 M NaCl). We infer that the chains are attached by strong local bonds. The flatly adsorbed fraction of the chains cannot escape into solution. Furthermore, this strong confinement prevents the chains from escaping the AFM tip and allows imaging of single chains.

Discussion

Large Length Scale. On large length scales (i.e., with a CP, radius approximately 3 μm), symmetric and asymmetric mea-

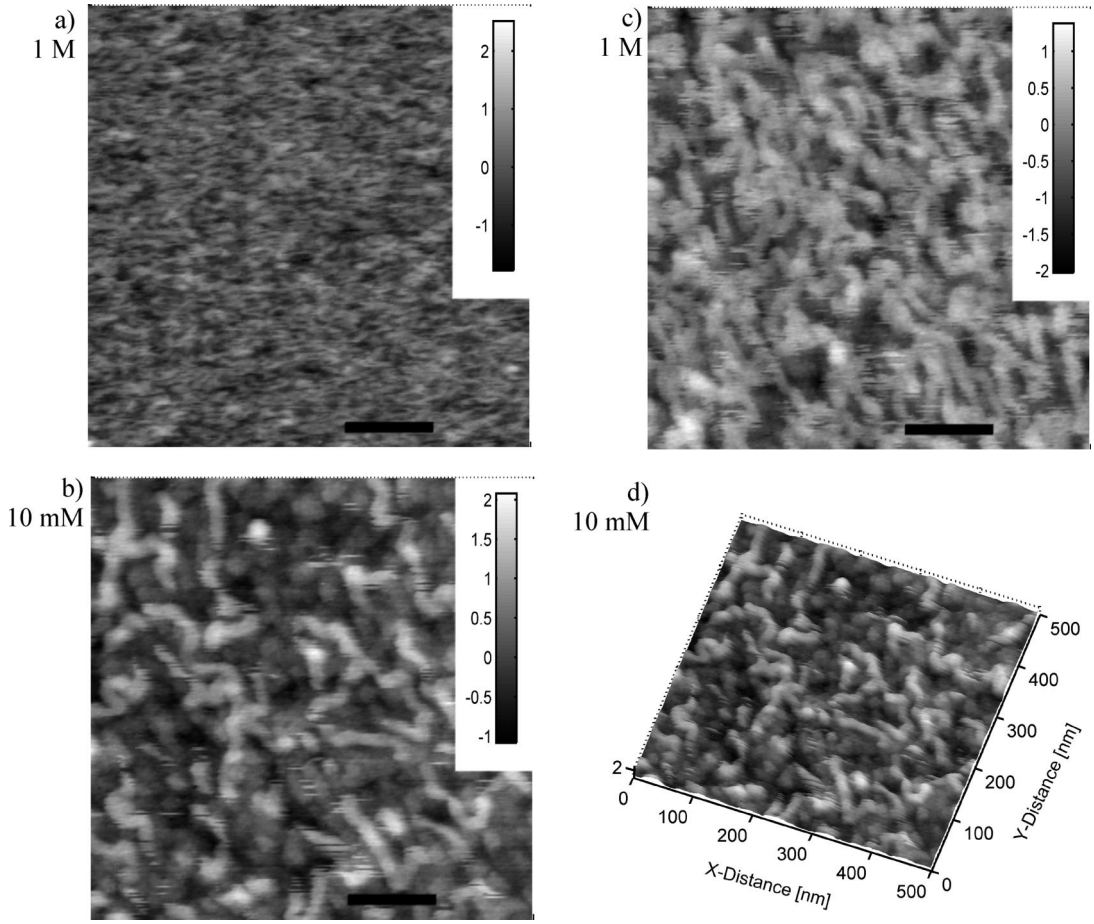

Figure 10. Tapping mode images of the PSS layer at diffent salt concentrations (scale bar represents 100 nm). The images (a) and (b) were recorded on a decrease of the salt concentration and image (c) after an increase to 1 M NaCl. Image (d) shows the data of (b) in a 3D plot. At 1 M NaCl (a) the surface appears homogeneous, and on decrease of the salt concentration (b) loops become visible which we attribute to single PSS chains adsorbed at the bottom of the brush. This change in surface structure is irreversible as indicated by (c), taken after increase back to 1 M NaCl. The brush itself is invisible to the AFM tip as the chains escape from the tip. The adsorbed chains are not much more stretched at 10 mM than at 1 M NaCl which indicates that they are attached by strong local bonds to the surface.

surements show that the PSS layer physisorbed from 1 M NaCl completely behaves like a salted and a neutral brush, respectively. The brush thickness scales as expected for salted polyelectrolyte brushes, and the dramatic changes in the brush thickness are attributed to the entropy of the incorporated ions. The force profiles are well described by the theories of Alexander, de Gennes, and Milner, Witten, and Cates which were derived for neutral end-grafted polymers.[15,19]

Both theories (although differing in the assumed volume fraction profiles) lead to similar force profiles and similar fit parameters, and deviations can only be observed below 10 mM NaCl where the brush thickness reaches one-third of the contour length. This means that above this concentration a difference between a boxlike (AdG) or parabolic (MWC) volume fraction profile cannot be resolved as the force profiles of both theories are numerically too similar.

The average pseudotail distance is found to be constant for both theories and all measurements and is on the order of 50 nm. From the assumption that one PSS chain (350 kDa) is located in the unit volume $L \cdot s^2$, one can cross-check the condition for the salted brush, $I_{NaCl} > I_{Mono}$,[34,35] which is found to be valid for $I_{NaCl} > 10$ mM. However, an order of magnitude deviation was found before and was attributed to counterion condensation, strong chain stretching, and the finite volume of monomers and hydrated ions.[40,41]

Additionally one can calculate a surface coverage s^{-2} of 0.2 mg/m^2 which is almost 1 order of magnitude less than reported in the literature.[12,42–44] This indicates that only a small fraction of the adsorbed PSS creates a steric interaction with the CP and that most of the adsorbed PSS is located inside or at the bottom of the brush. An indication of flat PSS adsorption is the charge overcompensation which occurred on PSS adsorption onto positively charged silane. Note that electrostatic force curves between the negatively charged AFM tip and surface are purely repulsive. This picture is further supported by tapping mode images which show a dense layer at the bottom of the brush.

We had to add an electrostatic contribution to the asymmetric force profiles to explain forces arising at surface separations where the steric force should vanish which resulted in a very good fit of the experimental data. Here we were able to measure the surface potential of the PSS brush. For these considerations, a crucial parameter is the surface potential of the bare silica CP as the asymmetric force profile depends on the product of this and the surface potential of the brush. We measured the CP surface potential independently, and the parameters are listed in Table S4 (in the Supporting Information). These values are in reasonable agreement with values reported in the literature.[20,42,45,46]

The values for the surface potential of the brush are also given in Table S4 and are located below 0.1 mV for all salt concentrations. We applied Grahame's equation[28]

$$\sigma = \sqrt{8\varepsilon\varepsilon_0 k_B T I_{NaCl}} \sinh(e\psi_{0,PSS}/2k_B T) \quad (8)$$

and calculated the surface charge of the PSS brush which is about 4.4 μC/m^2 (cf. right column in Table S4). This corresponds to one charge per 0.04 μm^2 or to an average charge distance of 150 nm (hexagonal grid) or 200 nm (Cartesian grid). This is on the same order of magnitude as the average pseudotail distance and would indicate that only every third or fourth brush exhibits one visible charge to the bare CP. This shows furthermore that the electrostatic force is very weak as the brush is almost perfectly neutralized by incorporated counterions.

By setting $\psi_{0,1} = \psi_{0,2} = \psi_{0,PSS}$ into eq 7, one can estimate the magnitude of the electrostatic force in symmetric measurements to be on the order of 0.01 pN which is 2 orders of magnitude less than the force resolution of 0.9 pN currently achievable by our setup. Hence, in symmetric measurements, electrostatic forces play no role, and deviations from the expected force profile may be due to deviations of the expected volume−fraction profile, polydispersity, or nonideal behavior of the layer.

However, zeta potential measurements show charge reversal after PSS adsorption onto silanized surfaces with potentials of about −40 mV.[1,47] Electrophoretic investigations provide information on the surface potential and the surface charge of particles. Yet, equally important for the interpretation of electrophoretic mobility data are the hydrodynamic properties of the outermost region of the interface. Zeta potential measurements rely on the different mobility of the anchored chains and the desorbed and associated counterions,[48] whereas with surface forces one measures the equilibrium distribution of the mobile counterions, not their hydrodynamic properties. Since we observe strong electrostatic repulsion between an AFM tip and the surface layer, we have evidence that the immobile part of the PSS layer, the flatly adsorbed chains, leads to surface charge reversal. The zeta potential relies on the mobility of the counterions within the brush and above the flat PSS layer, and there is a net negative surface charge even though it cannot be measured with probes on the micrometer scale but only with probes on the nanometer scale.

Small Length Scale. On a small length scale (AFM tip, curvature radius about 60 nm), the forces are best described by a linear superposition of a steric and an electrostatic contribution. The steric contribution is unexpected as the tip penetrates into the brush and as its magnitude is one order higher than expected (if calculated from the tip radius and Derjaguin's-approximation). Hence this force is caused by the interaction of the brush with the tip and also the tip stylus. The force profiles showed neither attractive forces nor adhesion but a strong electrostatic repulsion. Furthermore, tapping mode imaging showed a dense layer of PSS chains adsorbed on the surface.

Hence we conclude that the tip penetrates the brush (preventing the brush from being imaged) and interacts with the layer at the bottom of the brush. This is supported by previous measurements which showed that the brush can be imaged using a CP, but with a sharp AFM tip, no structural changes were observed on change of the salt concentration.[14]

However, we infer that the layer at the bottom of the brush acts as an anchor for the PSS chains protruding into solution. Without this anchoring layer, it is hard to explain why it is possible to reversibly swell and shrink the brush thickness by 1 order of magnitude without any hysteresis. Furthermore, this layer might be responsible for the possibility to dry the PSS layer and regain long-ranged forces in solution again. After drying, the brush will collapse but might be able to stretch again in solution if the osmotic pressure is high enough. A chain can stretch again into solution, if it collapses onto the flat PSS layer and not onto the positively charged silane surface. The bond between the flat PSS layer and the segments of the collapsed chain is weak.

An investigation of the degree of silanization, the surface coverage, and the behavior on drying will be a challenging task. We know little about the trains, tails, and loops. The observation of the flat chains which seem to be anchored at different surface points yet form loops into solution after exposure to diluted salt solutions suggests that some of the bonds between a PSS segment and the silanized surface are weak and can be dissolved by increased osmotic pressure in dilute salt solutions. Also, one has to consider cooperative effects. The separation of the pseudotails is fairly stable, therefore it is likely that each chain is anchored by a feasible fraction of the PSS chain.

Conclusion

By combining the information of asymmetric and symmetric measurements performed on two different length scales, we determined the conformation of the PSS layer physisorbed from 1 M NaCl solution: the PSS chains adsorb in a coiled conformation onto the silanized surface. Parts of the chains which are in contact to the oppositely charged surface form a dense and flat PSS layer, as was deduced from the repulsive electrostatic force found with the asymmetric tip measurements and from the AFM images. The latter show a uniform surface structure of silane and the PSS layer, respectively.

However, not all parts of the PSS chain adsorb onto the surface. These parts penetrate into solution and cause a long-range steric force which is investigated by force measurements with the CP. The chains are almost perfectly neutralized by counterions (leading to a very low surface potential, about 0.02−0.06 mV) and are subject to stretching as found in polyelectrolyte brushes. Hence, in symmetric force measurements, the electrostatic interaction manifests itself only in chain stretching, but not in an experimentally accessible surface potential.

Acknowledgment. We appreciate Wacker Chemtronic (Burghausen, Germany) for providing silicon wafers as a gift. This work was supported by the Deutsche Forschungsgemeinschaft (TR 24, project B7 and He 1616−9/4) as well as the state of Mecklenburg-Vorpommern.

Supporting Information Available: A table showing a comparison of parameters obtained by fits of the force profiles to the AdG and MWC theory, respectively (cf. Table S1). In that table, results of all four surface sets (S1, S2, S3, and S4) are given. After drying, the parameters of surface set S4 according to AdG theory are given (cf. Table S2). Also given are the parameters according to the AdG theory obtained from asymmetric force measurements, for surface S3 in Table S3a, and for surface S4 in Table S3b. The additional electrostatic parameters obtained from the asymmetric force measurements of surface S4 are given in Table S4. This material is available free of charge via the Internet at http://pubs.acs.org.

References and Notes

(1) Schönhoff, M. *Curr. Opin. Colloid Interface Sci.* **2003**, *8*, 86.
(2) Decher, G. *Science* **1997**, *277*, 1232.
(3) Caruso, F.; Caruso, R. A.; Möhwald, H. *Science* **1998**, *282*, 1111.
(4) Yoo, P. J.; Nam, K. T.; Qi, J. F.; Lee, S. K.; Park, J.; Belcher, A. M.; Hammond, P. T. *Nat. Mater.* **2006**, *5*, 234.
(5) Dubois, M.; Schönhoff, M.; Meister, A.; Belloni, L.; Zemb, T.; Möhwald, H. *Phys. Rev. E* **2006**, *74*, 051402.

(6) Hiller, J.; Mendelsohn, J. D.; Rubner, M. F. *Nat. Mater.* **2002**, *1*, 59.
(7) Holm, C.; Joanny, J. F.; Kremer, K.; Netz, R. R.; Reineker, P.; Seidel, C.; Vilgis, T. A.; Winkler, R. G. *Adv. Polym. Sci.* **2004**, *166*, 67.
(8) Netz, R. R.; Joanny, J. F. *Macromolecules* **1999**, *32*, 9026.
(9) Claesson, P. M.; Poptoshev, E.; Blomberg, E.; Dedinaite, A. *Adv. Colloid Interface Sci.* **2005**, *114*, 173.
(10) Lowack, K.; Helm, C. A. *Macromolecules* **1998**, *31*, 823.
(11) Kulcsar, A.; Voegel, J. C.; Schaaf, P.; Kekicheff, P. *Langmuir* **2005**, *21*, 1166.
(12) Cosgrove, T.; Obey, T. M.; Vincent, B. *J. Colloid Interface Sci.* **1986**, *111*, 409–418.
(13) Fleer, G. J.; Cohen Stuart, M. A.; Scheutjens, J.M.H.M.; Cosgrove, T.; Vincent, B. *Polymers at interfaces*; Chapman & Hall: London, 1993.
(14) Block, S.; Helm, C. A. *Phys. Rev. E* **2007**, *76*, 030801.
(15) de Gennes, P. G. *Macromolecules* **1980**, *13*, 1069.
(16) Claesson, P. M.; Dahlgren, M. A. G.; Eriksson, L. *Colloids Surf. A* **1994**, *93*, 293–303.
(17) Berndt, P.; Kurihara, K.; Kunitake, T. *Langmuir* **1992**, *8*, 2486–2490.
(18) Pericet-Camara, R.; Papastavrou, G.; Behrens, S. H.; Helm, C. A.; Borkovec, M. *J. Colloid Interface Sci.* **2006**, *296*, 496–506.
(19) Milner, S. T.; Witten, T. A.; Cates, M. E. *Macromolecules* **1988**, *21*, 2610–2619.
(20) Ducker, W. A.; Senden, T. J.; Pashley, R. M. *Langmuir* **1992**, *8*, 1831–1836.
(21) Butt, H. J.; Jaschke, M. *Nanotechnology* **1995**, *6*, 1–7.
(22) Sader, J. E.; Chon, J. W. M.; Mulvaney, P. *Rev. Sci. Instrum.* **1999**, *70*, 3967–3969.
(23) Cleveland, J. P.; Manne, S.; Bocek, D.; Hansma, P. K. *Rev. Sci. Instrum.* **1993**, *64*, 403–405.
(24) Papastavrou, G.; Kirwan, L. J.; Borkovec, M. *Langmuir* **2006**, *22*, 10880–10884.
(25) O'Shea, S. J.; Welland, M. E.; Rayment, T. *Langmuir* **1993**, *9*, 1826–1835.
(26) Butt, H. J.; Cappella, B.; Kappl, M. *Surf. Sci. Rep.* **2005**, *59*, 1–152.
(27) Derjaguin, B. V. *Kolloid Zeits.* **1934**, *69*, 155–164.
(28) Israelachvili, J. N. *Intermolecular and Surface forces*; Academic Press: London, 1991.
(29) Wang, L. X.; Yu, H. *Macromolecules* **1988**, *21*, 3498–3501.
(30) Odijk, T.; Houwaart, A. C. *J. Polym. Sci., Polym. Phys. Ed.* **1978**, *16*, 627–639.
(31) Nierlich, M.; Boue, F.; Lapp, A.; Oberthur, R. *Colloid Polym. Sci.* **1985**, *263*, 955–964.
(32) Essafi, W.; Lafuma, F.; Baigl, D.; Williams, C. E. *Europhys. Lett.* **2005**, *71*, 938–944.
(33) Qu, D.; Baigl, D.; Williams, C. E.; Möhwald, H.; Fery, A. *Macromolecules* **2003**, *36*, 6878–6883.
(34) Zhulina, E. B.; Birshtein, T. M.; Borisov, O. V. *Macromolecules* **1995**, *28*, 1491–1499.
(35) Netz, R. R.; Andelman, D. *Phys. Rep.* **2003**, *380*, 1–95.
(36) Balastre, M.; Li, F.; Schorr, P.; Yang, J. C.; Mays, J. W.; Tirrell, M. V. *Macromolecules* **2002**, *35*, 9480–9486.
(37) Tran, Y.; Auroy, P.; Lee, L. T. *Macromolecules* **1999**, *32*, 8952–8964.
(38) Butt, J. H. *Biophys. J.* **1991**, *60*, 1438–1444.
(39) Behrens, S. H.; Borkovec, M. *J. Phys. Chem. B* **1999**, *103*, 2918–2928.
(40) Ahrens, H.; Förster, S.; Helm, C. A.; Kumar, N. A.; Naji, A.; Netz, R. R.; Seidel, C. *J. Phys. Chem. B* **2004**, *108*, 16870–16876.
(41) Boroudjerdi, H.; Kim, Y. W.; Naji, A.; Netz, R. R.; Schlagberger, X.; Serr, A. *Phys. Rep.* **2005**, *416*, 129–199.
(42) Serr, A. Diploma Thesis, University of Geneva, Geneva, Switzerland, 2003.
(43) Schmitt, J. Ph.D. Thesis, Johannes Gutenberg Universität Mainz, Mainz, Germany, 1996.
(44) Ahrens, H.; Baltes, H.; Schmitt, J.; Möhwald, H.; Helm, C. A. *Macromolecules* **2001**, *34*, 4504–4512.
(45) Meagher, L.; Pashley, R. M. *Langmuir* **1995**, *11*, 4019–4024.
(46) Horn, R. G.; Smith, D. T.; Haller, W. *Chem. Phys. Lett.* **1989**, *162*, 404–408.
(47) von Klitzing, R. *PCCP* **2006**, *8*, 5012–5033.
(48) Donath, E.; Walther, D.; Shilov, V. N.; Knippel, E.; Budde, A.; Lowack, K.; Helm, C. A.; Möhwald, H. *Langmuir* **1997**, *13*, 5294–5305.

JP8020672